THE JOURNAL OF PHYSICAL CHEMISTRY LETTERS
A JOURNAL OF THE AMERICAN CHEMICAL SOCIETY

pubs.acs.org/JPCL

Letter

Revealing Brønsted Acidic Bridging SiOHAl Groups on Amorphous Silica−Alumina by Ultrahigh Field Solid-State NMR

Zichun Wang, Kuizhi Chen, Yijiao Jiang, Julien Trébosc, Wenjie Yang, Jean-Paul Amoureux, Ivan Hung, Zhehong Gan, Alfons Baiker, Olivier Lafon,* and Jun Huang*

Cite This: *J. Phys. Chem. Lett.* 2021, 12, 11563−11572

Read Online

ACCESS | Metrics & More | Article Recommendations | Supporting Information

ABSTRACT: Amorphous silica−aluminas (ASAs) are important acidic catalysts and supports for many industrially essential and sustainable processes. The identification of surface acid sites with their local structures on ASAs is of critical importance for tuning their catalytic properties but still remains a great challenge and is under debate. Here, ultrahigh magnetic field (35.2 T) ^{27}Al-{^{1}H} D-HMQC (dipolar-mediated heteronuclear multiple-quantum correlation) two-dimensional NMR experiments demonstrate two types of Brønsted acid sites in ASA catalysts. In addition to the known pseudobridging silanol acid sites, the use of ultrahigh field NMR provides the first direct experimental evidence for the existence of bridging silanol (BS: SiOHAl) acid sites in ASAs, which has been hotly debated in the past few decades. This discovery provides new opportunities for scientists and engineers to develop and apply ASAs in various reaction processes due to the significance of BS in chemical and fuel productions based on its strong Brønsted acidity.

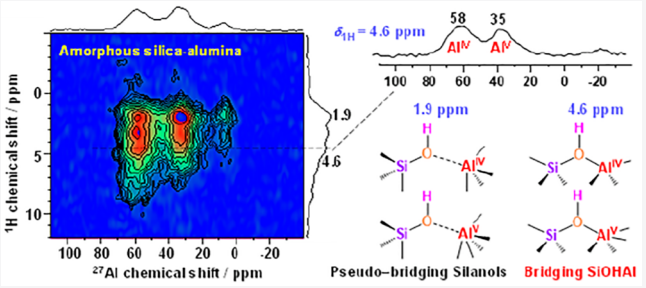

To realize green and sustainable energy and chemical productions, ecofriendly and cost-effective silica−alumina catalysts are extensively utilized for driving versatile acid-catalyzed hydrocarbon conversion reactions in drug and fine chemistry, petrochemical, and biorefining industries.[1,2] Compared to microporous zeolites, amorphous silica−aluminas (ASAs) offer unconstrained mass transfers and thus exhibit excellent performances in reactions involving large molecules as both acid catalysts and supports for metal active species. These properties render ASAs particularly interesting for applications in the conversion of biomass and derivatives for renewable energy and chemicals.[3−8] Moreover, ASAs are widely utilized in large-scale hydrocracking processes to balance the acidity for the selective production of middle distillates, such as diesel and kerosene fractions.[9]

So far, several models for the formation of catalytically active Brønsted acid sites (BASs) in ASAs have been proposed.[3,10−12] Two models are commonly considered for the formation of BASs on ASAs: (1) pseudobridging silanols (PBS: SiOH···Al)[3,13−15] with silanol groups tilting toward Al atoms with weak interaction; and (2) silanols weakly bounded to neighboring Al sites via electrostatic interactions.[16,17] In these models, there is no covalent bond between silanols and aluminum atoms. The acidic strength of these protons depends on Al sites coordinating to the hydroxyl oxygen of neighboring silanols as well as the SiOH···Al distance. Because of their amorphous nature, ASAs exhibit average SiOH···Al distances in the range of 2.94−4.43 Å, which are significantly longer than for bridging OH groups (SiOH-Al) in crystalline zeolites (1.88−2.0 Å).[13,14] These elongated SiOH···Al distances could weaken the polarization of the hydroxyl oxygens by neighboring Al sites, accounting for the much lower Brønsted acidity and catalytic performance of ASAs compared to zeolites.[18,19] In contrast, the weak acidity and poor activity of ASAs have been ascribed to the small amount of strong BASs existing in ASAs compared to zeolites.[20] The existence of strong BASs in ASAs has been reported by using reactivity measurements in propane cracking[21] and H/D exchange reactions.[22] Zeolite-like bridging SiOHAl acid sites in short-range order have also been proposed by theoretical calculations for the strong BASs in ASAs.[10] However, no direct spectral evidence has been reported so far for these strong BASs owing to their low density and their potentially broad signal due to their hydrogen-bond donor nature. Therefore, whether strong BASs are formed via PBS or SiOHAl, or both, is still strongly under debate.

Identifying the surface acid sites and their structure−property relationship is crucial for the rational design and performance optimization of ASAs. Various diffraction techniques, particularly X-ray diffraction (XRD), are powerful for studying the structure of crystalline zeolites. However, they fail to determine

Received: September 9, 2021
Accepted: October 22, 2021
Published: November 22, 2021

https://doi.org/10.1021/acs.jpclett.1c02975
J. Phys. Chem. Lett. 2021, 12, 11563−11572

unambiguously the local structures of ASAs due to their absence of long-range ordering, resulting in strong line broadening. IR spectroscopy could identify the surface sites but does not allow distinguishing between PBS and SiOHAl sites. Solid-state NMR spectroscopy is a powerful tool for characterizing surface acid sites and their local structures on silica−alumina materials.[19,23] In ^{1}H 1D spectra under magic-angle spinning (MAS), NMR signals at δ_{1H} = 1.2−2.2 ppm for PBS and terminal SiOH groups have been observed.[17,24,25] However, the signals at δ_{1H} = 3.6−5.2 ppm, typical for bridging SiOHAl acid sites in zeolites,[19] have never been detected so far. Indeed, even when suppressing the strong SiOH signal with a ^{1}H-{^{27}Al} TRAPDOR (transfer of population in double resonance) filter,[26,27] only the PBS signal at $\delta_{1H} \approx$ 1.8 ppm has been probed.[24]

The SENS-DNP technique (surface-enhanced NMR spectroscopy using dynamic nuclear polarization) can significantly enhance the ^{1}H sensitivity by 1 or 2 orders of magnitude.[28,29] It has been used on ASAs, but still, no SiOHAl sites could be detected.[14] The analysis of the dephasing curves obtained from DNP-enhanced ^{17}O-{^{27}Al} TRAPDOR experiments have shown that in ASAs the average distances between Al and neighboring SiOH groups are well in line with the theoretical value of PBS.[14] In the same work, compared to PBS at δ_{1H} = 1.3 ppm the signal at δ_{1H} = 5 ppm correlates with ^{17}O nuclei as well, but is characterized with slower dephasing in ^{17}O-{^{27}Al} TRAPDOR experiments. This hints at a significantly longer distance between Al−O for the OH signal at δ_{1H} = 5 ppm, and hence, it was assigned to hydrogen-bonded OH groups other than bridging OH groups. Therefore, the direct observation of SiOHAl on ASAs remains a great challenge.

^{27}Al-{^{1}H} D-HMQC (dipolar-mediated heteronuclear multiple-quantum correlation between ^{27}Al and ^{1}H with ^{27}Al observation) two-dimensional (2D) NMR experiments provide information on ^{1}H−^{27}Al proximities.[15,30] This experiment has notably allowed the observation of PBS sites at B_0 = 18.8 T on the surface of ASAs. Recently, an ^{27}Al-{^{1}H} D-HMQC experiment at B_0 = 20.0 T has been applied to detect the acid sites of aluminum oxide films grown on a silica support.[31] A very broad signal centered at δ_{1H} = 4.3 ppm was obtained from the simulation of the indirect ^{1}H dimension of the ^{27}Al-{^{1}H} D-HMQC spectra, but the indirect ^{1}H dimension of the corresponding ^{29}Si-{^{1}H} spectra shows only a strong signal at δ_{1H} = 2.5 ppm without a signal at δ_{1H} = 4.3 ppm. Therefore, it is still under debate whether the broad signal at δ_{1H} = 4.3 ppm is due to the presence of bridging SiOHAl groups or mainly a combination of various bridging AlOHAl groups.[32]

Here, we report that this experiment carried out at the ultrahigh magnetic field of B_0 = 35.2 T provides direct evidence for the presence of bridging SiOHAl acid sites on the surface of ASAs. To the best of our knowledge, these sites have never been observed directly so far. This detection is possible since higher B_0 fields increase the resolution along both ^{1}H and ^{27}Al dimensions and thus allow identifying sites that are undetectable at lower magnetic fields.[30] This is particularly the case of ^{27}Al nuclei bonded to bridging OH groups, which are broadened by large quadrupole interactions and hence which are largely "invisible" at magnetic fields up to 18.8 T.[27,33] Conversely, the reported ^{27}Al-{^{1}H} D-HMQC spectra at 35.2 T allow resolving a new correlation signal between tetracoordinated Al (Al^{IV}) species (δ_{27Al} = 55−58 ppm) and bridging OH groups (δ_{1H} = 4.6 ppm), demonstrating the presence of bridging silanol groups linked to Al. A similar correlation is also first observed with pentacoordinated Al (Al^{V}) species (δ_{27Al} = 31−35 ppm), revealing the formation of SiOHAl BASs based on Al^{V} species, which have never been probed hitherto. Moreover, we demonstrate that the SiOHAl formation and the distribution of Al species in ASAs depend on the Al/Si ratio. The detailed insights into surface acid sites and the discovery of new SiOHAl in ASAs pave the way for generating strong SiOHAl in ASAs, which facilitates the optimization of their performance for acid catalysis and multifunctional catalysis in various fields.

ASA catalysts were prepared within microseconds at an extremely high temperature (ca. 2000 K) by the flame-spray pyrolysis (FSP) technique.[34] Aluminum(III) acetylacetonate (99%, ABCR), tetraethoxysilane (99%, Fluka), acetic acid (analytical grade, Fluka), and methanol (analytical grade, Fluka) were used as received. In brief, the appropriate amounts of the Al and Si precursor materials were dissolved in a 1:1 (vol) mixture of acetic acid and methanol. The resulting solution was filtered using a glass filter, pumped through a capillary at a rate of 5 mL·min^{-1}, nebulized by using an O_2 flow rate of 5 L·min^{-1}. The resulting spray was ignited by an annular supporting methane/oxygen flame (1.5/0.9 L·min^{-1}) to generate ASA nanoparticles with a large amount of Al^{V} species. The ASA samples with different atomic ratios of Al/Si are designated as ASA/X, where X represents the percentage of Al atoms with respect to the total amount of Al and Si atoms in the precursors. The nitrogen isotherms, specific surface areas, concentrations of OH groups, and densities of BAS and Lewis acid sites (LAS) of these ASA materials were determined in our previous works.[5,34,35]

All 2D NMR experiments were performed on the 35.2 T (^{1}H 1.5 GHz) Series-Connected Hybrid (SCH) magnet operated at the National High Magnetic Field Laboratory (NHMFL, Tallahassee, USA), equipped with a Bruker Avance NEO console. A 2.0 mm triple resonance probe designed and built at the NHMFL was used in double resonance mode and with a sample spinning frequency of ν_R = 30 kHz. The ^{1}H and ^{27}Al isotropic chemical shifts were referenced indirectly by using a D_2O sample at room temperature (^{17}O δ_{iso} = −2.8 ppm) and the IUPAC reference sample frequencies in ref 36.

The ^{27}Al triple-quantum magic-angle spinning (3QMAS) spectra of ASAs were recorded with a shifted-echo pulse sequence[37] and sheared with the QSHEAR program using Matlab.[38] Excitation and reconversion pulses lasted t_p = 3.75 and 1.25 μs, respectively, with a radiofrequency (rf) field strength of ν_1 = 96 kHz and central-transition (CT) selective $\pi/2$ and π pulses of 10 and 20 μs at ν_1 = 8.3 kHz. The 2D 3QMAS spectra were acquired with complex acquisition using Δt_1 = 33.33 μs, NS = 1920 transients, 20 t_1 increments, and a recovery delay T_{RD} = 0.1 s.

Proximities between ^{27}Al nuclei were probed using 2D ^{27}Al through-space double-quantum to single-quantum (DQ-SQ) homonuclear correlation experiments using $\pi/2$ and π-pulses of 10 and 20 μs CT-selective with ν_1 = 8.3 kHz. The ^{27}Al two-spin DQ coherences were excited and reconverted by applying the $BR2_2^1$ pulse sequence,[39] which reintroduces the ^{27}Al−^{27}Al dipolar interactions under MAS. The lengths of the excitation and reconversion times were optimized on ASA/50 as $\tau_{exc} = \tau_{rec}$ = 800 μs. The rf amplitude applied during the $BR2_2^1$ pulse sequence was 5 kHz, which corresponds to a nutation frequency of 15 kHz for the ^{27}Al CT, which matches the HORROR (homonuclear rotary resonance) condition. Furthermore, a WURST (wideband, uniform rate, smooth truncation) adiabatic pulse with a frequency sweep equal to the MAS frequency and an offset of 300 kHz with respect to the CT was applied before the $BR2_2^1$ excitation,[40] to enhance the ^{27}Al CT polarization by

https://doi.org/10.1021/acs.jpclett.1c02975
J. Phys. Chem. Lett. 2021, 12, 11563−11572

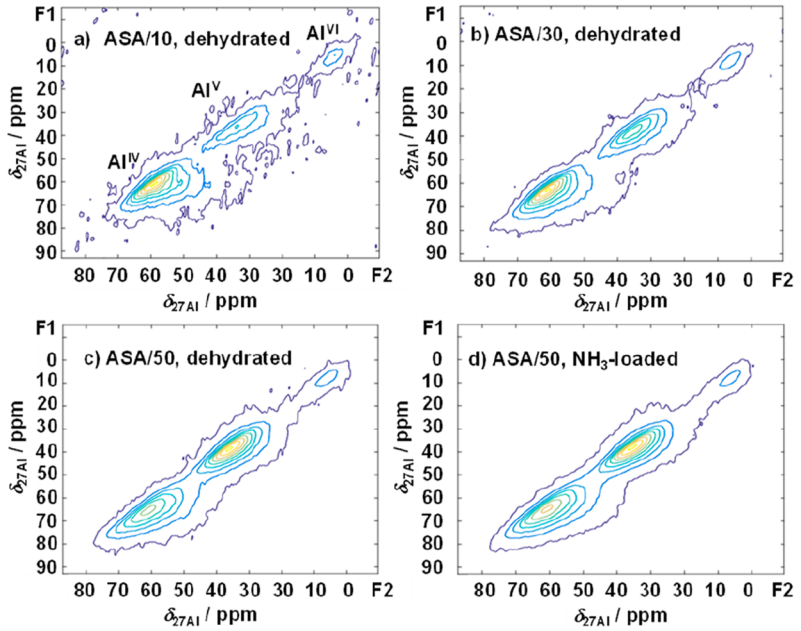

Figure 1. ^{27}Al 3QMAS ASA spectra recorded at 35.2 T with ν_R = 30 kHz of (a) ASA/10, (b) ASA/30, and (c) ASA/50, dehydrated at 723 K under a vacuum for 12 h, as well as (d) ASA/50 loaded with ammonia and evacuated at 373 K for 1 h.

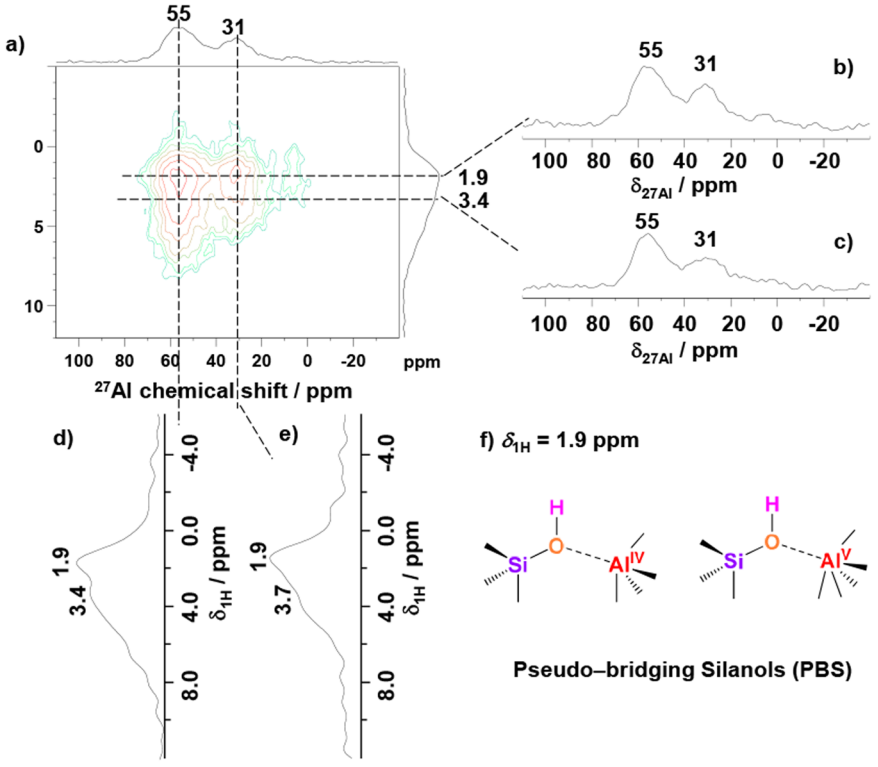

Figure 2. Correlation spectra of dehydrated ASA/10. (a) 2D ^{27}Al-{^{1}H} D-HMQC spectrum acquired using τ_{rec} = 3.2 ms, along with the ^{27}Al and ^{1}H 1D slices displayed in panels (b, c) and (d, e), respectively. (f) Proposed structure of PBSs corresponding to the dominant cross-peaks in the ^{27}Al-{^{1}H} D-HMQC spectrum. ASA/10 was dehydrated at 723 K for 12 h under a vacuum, and the spectra were recorded at 35.2 T with ν_R = 30 kHz.

inverting/saturating the satellite transitions.[41,42] The 2D ^{27}Al DQ-SQ spectra resulted from averaging 2048 transients for ASA/10 and ASA/30, and 3072 transients for ASA/50, respectively, with Δt_1 = 33.33 μs, 20 t_1 increments, T_{RD} = 0.1 s, resulting in a total experimental time of 2.5 and 3.75 h, respectively.

To enhance the sensitivity, the ^{27}Al nuclei were observed since its rapid longitudinal relaxation allows the use of short recovery delays. The ^{1}H−^{27}Al dipolar couplings were reintroduced by applying an SR4$_1^2$ recoupling on the ^{1}H channel.[43] The ^{1}H rf amplitudes for the 90° pulses and the SR4$_1^2$ recoupling were equal to $\nu_1 \approx$ 60 kHz. The CT-selective pulse lengths on ^{27}Al were equal to 10 and 20 μs for $\pi/2$ and π pulses, respectively, i.e.,

https://doi.org/10.1021/acs.jpclett.1c02975
J. Phys. Chem. Lett. 2021, 12, 11563−11572

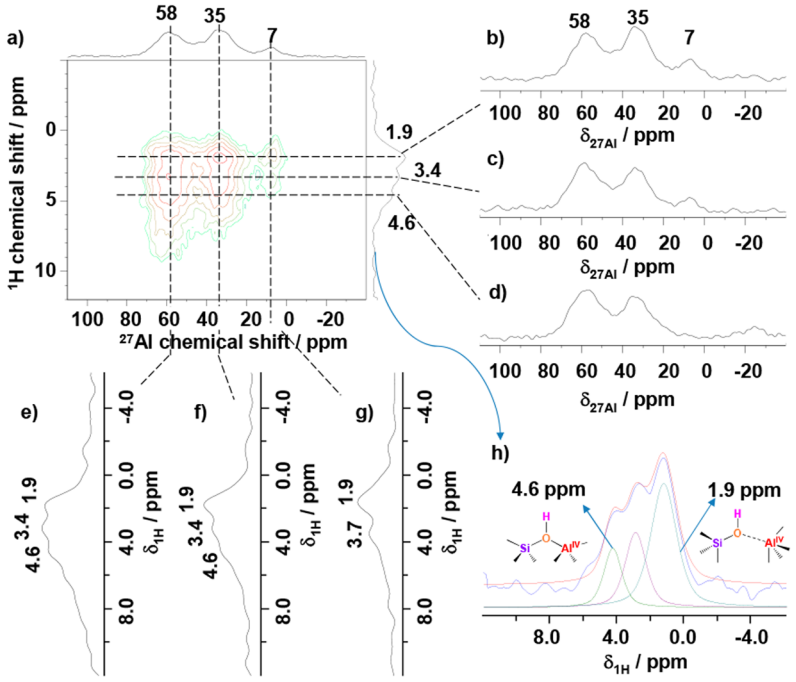

Figure 3. Correlation spectra of dehydrated ASA/30. (a) ^{27}Al-{^{1}H} D-HMQC 2D spectrum acquired using τ_{rec} = 3.2 ms, along with the ^{27}Al and ^{1}H 1D slices displayed in panels (b−d) and (e−g), respectively. (h) Simulation of the ^{1}H projection of (a) and the proposed local environments of silanol groups based on spectrum (a) and corresponding slices. ASA/30 was dehydrated at 723 K for 12 h under a vacuum, and spectra were recorded at 35.2 T with ν_R = 30 kHz.

an rf-field amplitude ν_1 = 8.3 kHz. The total dipolar recoupling time was optimized at τ_{rec} = 3.2 ms. The 2D spectra resulted from the accumulation of NS = 1024 transients with States-TPPI acquisition of 16 complex t_1 increments with Δt_1 = 33.33 μs and T_{RD} = 0.1 s, i.e., a total experiment time of about 1 h.

The formation of BASs strongly depends on the coordination number of Al species in dehydrated ASAs, which could be determined at 35.2 T from 1D MAS (Figure S1 in Supporting Information) and 2D 3QMAS ^{27}Al NMR spectra (Figure 1). The 2D 3QMAS spectra of these catalysts are dominated by the Al^{IV} and Al^{V} signals, while a weaker signal ascribed to hexacoordinated Al sites (Al^{VI}) is also visible, in agreement with previous reports.[15,44] Then the simulations of corresponding 1D ^{27}Al MAS NMR spectra were performed. The obtained quadrupole parameters and concentration of each Al species are summarized in Table S1. With an increasing Al/Si ratio from 10/90 to 30/70 and 50/50, called ASA/10, ASA/30, and ASA/50, the content of Al^{V} is remarkably raised. The high temperature and fast cooling rate under oxygen-rich atmosphere could promote the generation of intermediate Al^{V} species in ASAs, which may be caused by the local structure reformation under the harsh synthesis conditions.[3,24,45]

Unlike bridging OH groups on zeolites,[46] only a slight decrease of quadrupole coupling constant (C_Q) was detected for ASA/50 before and after ammonia loading (Table S1). A direct comparison of their 1D ^{27}Al MAS NMR spectra (Figure S1e) shows an increase of the ^{27}Al signal intensity with small line narrowing. In zeolites, a significant line narrowing for bridging OH groups could be observed even at a magnetic field of 9.4 T. This reduced effect is attributed to the wide chemical shift distribution of Al sites in ASA compared to those in crystalline zeolites. Furthermore, for PBS on ASAs, the ammonia loading has a limited effect on the ^{27}Al spectra recorded at a magnetic field of 16.4 T,[15] which is attributed to the much longer Al−OH distance than in zeolites. The effect upon ammonia loading of the possible bridging SiOHAl groups in ASA could be masked by the signals of other Al sites. Therefore, ^{27}Al-{^{1}H} D-HMQC 2D NMR experiments were applied to probe selectively the surface protons in connection with Al sites.

In ASA/10, the dominant Al^{IV} and Al^{V} species are highly dispersed in the silica networks on the surface,[44] which is proposed to promote the formation of moderate BASs.[15] ^{27}Al-{^{1}H} D-HMQC 2D spectra at $B_0 \leq$ 18.8 T only exhibit a broad ^{27}Al signal at 60−20 ppm correlated to the ^{1}H signal at 1.9 ppm (see Figure S2). When the width of the ^{27}Al resonance is dominated by the second-order quadrupolar interaction, the resolution of the ^{27}Al 1D spectra is proportional to $(B_0)^2$ and hence is improved at higher magnetic fields. Here, cross-peaks between both Al^{IV} (δ_{27Al} = 55 ppm) and Al^{V} (δ_{27Al} = 31 ppm) species interacting with neighboring SiOH groups (δ_{1H} = 1.9 ppm) are clearly resolved at B_0 = 35.2 T (Figure 2b) and confirmed by the corresponding ^{27}Al 1D slices (Figures 2d,e). These cross-peaks are ascribed to PBSs generated in ASA/10 (Figure 2f), responsible for the moderate Brønsted acidity of ASAs with low Al/Si ratios. Moreover, an additional weak ^{1}H signal at δ_{1H} = 3.4 ppm that correlates with both Al^{IV} and Al^{V} species (Figure 2a,c) has been assigned to AlOH groups.[19] Since terminal AlOH groups are often observed at δ_{1H} shifts ranging from −0.5 to 0.7 ppm, the strong observed deshielding indicates that these AlOH are either polarized by neighboring sites or bridged to other Al sites, as in doubly bridging (μ_2) AlOHAl sites.[19,47] The ^{27}Al DQ-SQ 2D spectrum of ASA/10 (Figure S3a) exhibits Al^{IV}−Al^{IV}, Al^{IV}−Al^{V}, and Al^{V}−Al^{V} correlations, which were undetectable in previous works at 18.8 T due to their low concentration and strong line broadening.[3] Since no strong BASs could be detected in ASA/10,[34] these proximities between Al sites are not accompanied by a significant synergistic effect on the same SiOH group.[3] The detected proximities between Al

https://doi.org/10.1021/acs.jpclett.1c02975
J. Phys. Chem. Lett. 2021, 12, 11563−11572

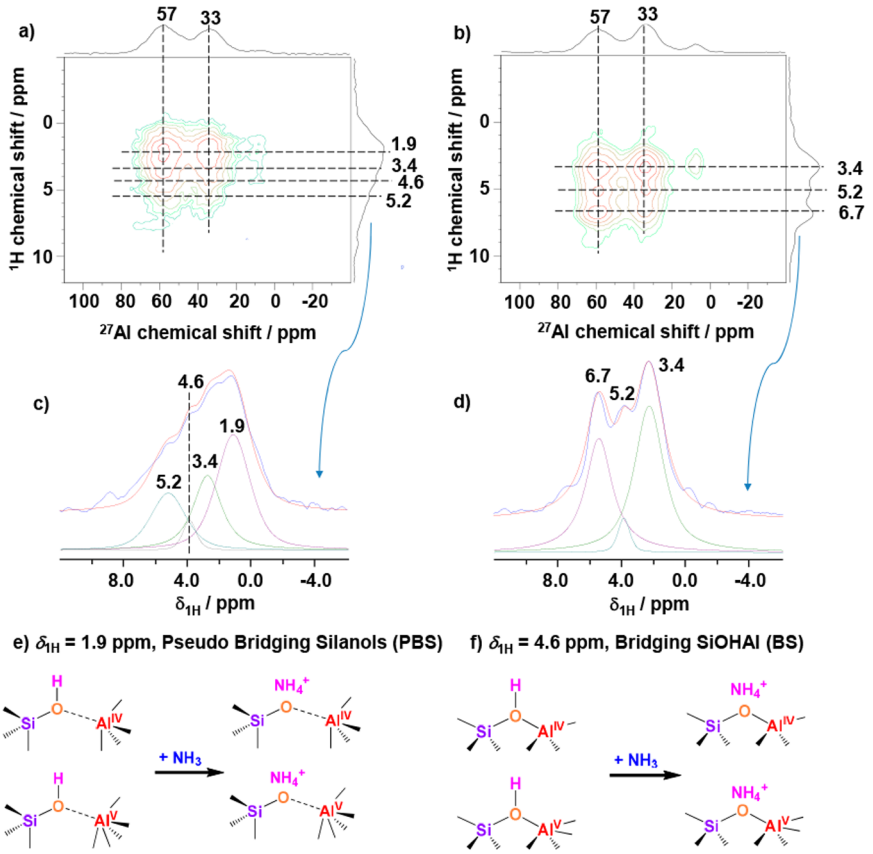

Figure 4. ^{27}Al-{^{1}H} D-HMQC spectra of ASA/50: (a) dehydrated at 723 K for 12 h under a vacuum and (b) upon ammonia loading. (c, d) Simulation of the ^{1}H projection of (a) and (b). (e, f) Proposed structures of PBS and BS sites before and after their reaction with ammonia. Spectra were recorded at 35.2 T with ν_R = 30 kHz and τ_{rec} = 3.2 ms.

sites are proposed to be existing in a few nearby Al species, requiring AlOH groups to balance the local structure as supported by DFT calculation studies.[44] These AlOH groups produce a deshielded ^{1}H signal at δ_{1H} = 3.4 ppm. In addition to the SiOH···Al^{IV} sites, the presence of Al^{IV}−O−SiOH species has been suggested by DFT calculations from the silication of the (100) γ-Al_2O_3 surface,[48] which could be centered at δ_{1H} = 1.9 ppm as well. After loading with NH_3, the ^{1}H peak of acidic SiOH···Al^{IV} sites is shifted to ca. 6.7 ppm for NH_4^+, while the ^{1}H peak of nonacidic Al^{IV}−O−SiOH species remains at around 1.9 ppm. Upon NH_3 loading, the ^{1}H peak at 1.9 ppm in Figure 2a disappeared and was replaced by a peak at δ_{1H} = 6.7 ppm,[15] demonstrating the absence of Al^{IV}−O−SiOH species.

At a higher Al concentration, besides the signals of moderate BASs and AlOH groups at δ_{1H} = 1.9 and 3.4 ppm, an additional signal at δ_{1H} = 4.6 ppm was detected in dehydrated ASA/30 (Figure 3a). Physisorbed and hydrogen-bonded water molecules on ASAs show ^{1}H signals at ca. δ_{1H} = 4.6−4.8 ppm, which could be probed by ^{1}H MAS NMR even at low magnetic fields (7.0 T).[49] However, these signals are undetectable in ^{1}H DQ-SQ 2D spectra at 18.8 T for dehydrated ASAs as used here.[3] Hence, the presence of water molecules with signals at δ_{1H} = 4.6 ppm can be ruled out. The formation of bridging AlOH groups at similar ^{1}H chemical shifts (δ_{1H} = 3−4.5 ppm) has been reported recently for Al_2O_3 at 35.2 T.[47] On the other hand, the signal at δ_{1H} = 4.6 ppm is typical for bridging OH groups in crystalline zeolites.[32]

In ASAs, BASs originate from Al^{IV} or Al^{V} sites interacting with neighboring SiOH groups in the alumina-silica interphase region or inside the silica networks, whereas Al^{VI} species are typically in the alumina phase and do not contribute to the formation of BASs. The ^{27}Al DQ-SQ 2D spectrum of dehydrated ASA/30 (Figure S3b) does not exhibit any correlation with the Al^{VI} signal, suggesting that no significant alumina phase exists in ASA/30, which is in line with a previous report.[44] The D-HMQC spectrum shows cross-peaks between Al^{VI} species (δ_{27Al} = 7 ppm) and either SiOH (δ_{1H} = 1.9 ppm) or bridging AlOH (δ_{1H} = 3.4 ppm) groups (see the slices shown in Figures 3b,c,g). The NMR observations suggest that some Al^{VI} species are isolated on the silica surface, whereas other ones are located in the proximity of AlOH groups in Figures 3c,g. However, the Al^{VI} species are not in connection with the signal at δ_{1H} = 4.6 ppm in ASA/30 (Figure 3d), demonstrating that this signal (δ_{1H} = 4.6 ppm) is not associated with the alumina phase. The signal at δ_{1H} = 4.6 ppm mainly correlates with Al^{IV} or Al^{V} signals and thus is considered to be located either in the alumina-silica interphase region or inside the silica networks, contributing to BASs (Figure 3h).

Similar structures are also detected for ASAs with higher Al/Si ratios (Figure 4). However, the signals at δ_{1H} = 4.6 and 3.4 ppm are overlaid by the intense one at δ_{1H} = 1.9 ppm in the ^{27}Al-{^{1}H} D-HMQC 2D spectrum of dehydrated ASA/50 (Figure 4a). The cross-peaks between Al^{IV} and Al^{V} sites and the ^{1}H signal at 1.9 ppm are ascribed to PBSs interacting with one or two nearby Al atoms.[3,15] The first case leads to moderate BASs, which can catalyze the dehydration of cyclohexanol.[6] However, we have recently shown that the presence of an additional Al atom in the vicinity of PBSs can enhance their Brønsted acidity.[3] This

https://doi.org/10.1021/acs.jpclett.1c02975
J. Phys. Chem. Lett. 2021, 12, 11563−11572

increased intensity of the ^{1}H signal at 1.9 ppm at a high Al/Si ratio indicates an increased amount of PBSs, which is consistent with a homogeneous distribution of Si atoms into the alumina matrix or on the alumina surface of ASAs at high Al/Si ratios.[13,14]

The D-HMQC 2D spectrum of dehydrated ASA/50 shown in Figure 4a exhibits cross-peaks between Al^{IV} and Al^{V} sites and the ^{1}H signal at δ_{1H} = 5.2 ppm. This ^{1}H chemical shift has been ascribed to aluminols, bridging OH groups, or hydrogen-bonded hydroxyls.[19] Similar to bridging AlOH groups observed at δ_{1H} = 3.4 ppm (Figures 2c, 3c, and S4b), the OH groups at δ_{1H} = 5.2 ppm is in proximity to Al^{VI} species, but the chemical shift is significantly higher than that of triply bridging AlOH groups in alumina resonating at δ_{1H} = 3.4 ppm.[47] Hence, the cross-peaks at δ_{1H} = 5.2 ppm could be ascribed to triply bridging AlOH in strong electrostatic interaction with neighboring oxygen atoms, similar to hydrogen-bonded hydroxyls observed in zeolites[19] or AlOH groups, which are hydrogen-bond donors.[50]

The acidic properties of surface protons could be identified using NH_3 as probe molecule because the protonation of NH_3 at BASs results in NH_4^+ ions producing a ^{1}H signal at δ_{1H} = 6.5−7.0 ppm, which can clearly be distinguished from other OH groups in silica−aluminas. NH_3 coordinated to Lewis acidic Al sites on Al_2O_3 and ASA leads to ^{1}H signals in the range δ_{1H} = −0.5 to 4.6 ppm.[35,51−53] AlOH groups are generally inactive in protonating NH_3. Although a recent report shows protonation of NH_3 on Al_2O_3, the amount of potential acidic OH groups is very small compared to LASs.[51] Since AlOH groups are inactive for the protonation of ammonia, the increase in the signal intensity of the cross-peaks between Al^{V} resonance and ^{1}H signals at 3.4 and 5.2 ppm upon ammonia loading is attributed to the adsorption of ammonia at LASs (Figures S4b,g,d,h).[35] In the ^{27}Al-{^{1}H} D-HMQC 2D spectrum shown in Figure 4b, the cross-peaks at δ_{1H} = 1.9 and 4.6 ppm have disappeared compared to Figure 4a, while concomitantly a signal at δ_{1H} = 6.7 ppm appears. The large intensity of the ammonium signal and the very limited change in the signals of AlOH groups (Figures S4b,g,h) indicate that the proton donation arises mainly from the peaks at δ_{1H} = 1.9 and 4.6 ppm. These spectral modifications demonstrate that these two proton species are surface BASs. The complete deprotonation (disappearance) of the peak at δ_{1H} = 1.9 ppm in Figure 4b is because mainly acidic SiOH groups with neighboring Al centers can be selectively detected in ^{27}Al-{^{1}H} D-HMQC experiments, while nonacidic SiOH groups are still observed upon ammonia adsorption using conventional ^{1}H 1D experiments (Figure S5).[15,34] The signal at δ_{1H} = 1.9 ppm is widely accepted for PBS sites in ASAs. DFT calculations show that the interaction between SiOH groups and local Al sites in ASAs is very weak compared to bridging SiOHAl groups, unless deprotonation upon adsorption of probe molecules occurs.[54] Therefore, both moderate and strong PBS sites denote similar signals at δ_{1H} = 1.9 ppm, without strong deshielding on the nearby silanol protons. Therefore, the signal at δ_{1H} = 4.6 ppm does not arise from the PBS and the bridging AlOH in alumina phase. The acidic hydroxyl groups with δ_{1H} = 4.6 ppm can correlate with Al^{IV} and Al^{V} sites (Figures S4c,e,f,j,k). In zeolites, Al^{IV} sites lead to a significant deshielding of the ^{1}H resonance on neighboring OH groups, like in bridging $SiOHAl^{IV}$ groups. Therefore, the cross-peaks between the signal at δ_{1H} = 4.6 ppm and Al^{IV} and Al^{V} peaks are ascribed here to bridging $SiOHAl^{IV}$ and $SiOHAl^{V}$ moieties. These two groups transfer protons to ammonia. To the best of our knowledge, $SiOHAl^{V}$ acid sites have never been observed so far.

As the heteronuclear coherence transfers in ^{27}Al-{^{1}H} D-HMQC experiments are only effective up to a few Å, the ^{1}H signal of ammonium ions only correlates with ^{27}Al signals involved in the conjugated base of BASs. Hence, the cross-peaks of the ^{1}H signal of ammonium ions in D-HMQC spectra demonstrate that BASs contain both Al^{IV} and Al^{V} sites. The structures of PBS and BS involving Al^{IV} and Al^{V} sites and their reactions with ammonia are shown in Figures 4e,f. Both PBS and BS act as BASs. To determine the population densities of BASs based on PBS and BS, we assume that they have comparable transfer efficiencies in the D-HMQC experiments. Then the population densities of PBS and BS are determined from the integrated intensities of their signal in the ^{1}H projection of D-HMQC spectra (Figures 3h and 4c,d), and the as-derived molar fractions are given in Table 1. The fraction of SiOHAl amounts to the range of 9.2−24% of the total number of BASs, and PBS are predominant in ASAs. With an increasing Al/Si ratio from 30/70 to 50/50, the molar fraction and the number of SiOHAl were significantly reduced.

Table 1. Molar Fraction and Concentration of BS and PBS BASs on ASAs[a]

	molar fraction of BS[b]/%	density of BS/ mmol/g	density of PBSs/mmol/g
ASA/10	0	0	9.8×10^{-2}
ASA/30	18.3	2.0×10^{-2}	9.1×10^{-2}
ASA/50	9.2	1.2×10^{-2}	12.2×10^{-2}

[a]Total densities of BASs in ASAs were obtained from ref 34. [b]Molar fractions of BS were determined by the ratios (BS)/(BS + PBS) of the integrated intensities obtained from simulations of the ^{1}H projections of ^{27}Al-{^{1}H} D-HMQC 2D spectra of dehydrated ASA.

Bridging OH groups are widely accepted to be generated based on framework Al^{IV} species in crystalline zeolites but are rarely probed in ASAs. Generally, Al^{IV} species involved in $SiOHAl^{IV}$ groups are subject to very large C_Q values, e.g., up to 15 ± 1 MHz for framework Al^{IV} species in zeolite H−Y,[33] causing significant line broadening, and thus are "invisible" at low to medium magnetic fields. Increasing the magnetic field strength and the spinning rate may significantly narrow the ^{27}Al signal and allow recovering this "invisible" signal. Moreover, ^{27}Al-{^{1}H} D-HMQC 2D spectra allow the selective detection of SiOH groups with different neighboring Al sites, while removing the ^{1}H signal of nonacidic terminal SiOH groups.

With this in mind, the newly observed signals at δ_{1H} = 4.6 ppm in proximity to Al^{IV} species demonstrate the formation of SiOHAl groups in ASAs, which are similar to those observed in zeolites with the same ^{27}Al-{^{1}H} D-HMQC 2D experiments.[30] These ^{27}Al and ^{1}H correlations are undetectable when using a magnetic field of 18.8 T (Figure S2) but could be detected at 35.2 T. This observation confirms that these Al species are subject to large quadrupole interactions. Large values of C_Q = 13−16.6 MHz, similar to those reported for framework Al^{IV} species, have been calculated in ASAs by DFT calculations for Al^{IV} with neighboring silanols.[44] These SiOHAl environments of ASAs exhibit similar ^{1}H chemical shifts and acidic properties as bridging OH groups in zeolites.

More interestingly, Al^{V} species exhibit similar proximity to bridging OH groups at δ_{1H} = 4.6 ppm, as observed with Al^{IV} species. Al^{V} species interacting with SiOH groups can exhibit C_Q ≈ 12−16 MHz, according to DFT calculations,[44] similar to those reported for framework Al^{IV} species in zeolite H−Y.[33]

https://doi.org/10.1021/acs.jpclett.1c02975
J. Phys. Chem. Lett. 2021, 12, 11563−11572

^{27}Al-{^{1}H} D-HMQC 2D spectra, recorded before and after ammonia loading (Figures 4a,b), demonstrate that Al^{V} species are in proximity to protons at δ_{1H} = 4.6 ppm and ammonium ions (Figure S4f,k) and are thus acting as SiOHAl. The cross-peaks with the Al^{V} signal in D-HMQC 2D spectra have intensities similar to those with Al^{IV} resonance (Figures 3d and S4c). Therefore, bridging sites interacting with Al^{V} sites represent a significant fraction of the total amount of the bridging sites and not only some extra sites in the structure. Furthermore, the reaction of ASAs with ammonia (Figure 4b) indicates that Al^{IV} and Al^{V} are unsaturated species with similar properties to promote the acid strength of neighboring silanols (δ_{1H} = 1.9 ppm).

The formation of bridging SiOHAl groups in ASAs has been proposed by DFT calculation studies, constructed from the silication of the (100) γ-Al_2O_3 surface upon hydrothermal treatment.[10,13,54,55] The presence of bridging SiOHAl groups requires a high hydroxyl coverage (≥5.4 OH nm^{-2}),[13] much higher than that (ca. 2.8−3.0 OH nm^{-2}) on flame-made ASAs.[34] In the DFT model, the bridging SiOHAl groups are formed based on Al^{V} species, other than the well-accepted Al^{IV} species in zeolites.[55] However, SiOHAl groups based on both Al^{IV} and Al^{V} species are observed in this work. The DFT-derived structural parameters of SiOHAl groups in ASAs are like those reported for zeolites, such as bond distances (Al−O, Si−O, and O−H) and Si−O−Al angle.[13] With the similar structure, similar large C_Q values of SiOHAl in ASAs and zeolites can be expected and are reported in DFT calculation studies as discussed above.[44] Therefore, our observations of SiOHAl groups in ASAs can be supported by the existing DFT calculation studies.

To the best of our knowledge, the bridging silanol groups $SiOHAl^{V}$ have never been reported experimentally so far, and the above results represent the first direct observation of bridging silanol groups in ASAs, in which a PBS local environment dominates. These observations well support the strong BASs probed in ASAs in previous works.[20−22] The formation of BS could depend on the wide distribution of Al species in ASAs, leading to BASs with versatile strengths and structures. For ASAs prepared at milder conditions, mainly moderate BASs based on Al^{IV} sites are generated, and thereby observing directly the structure of a few strong BASs is quite difficult. Likewise, distinguishing the structure of strong BASs from PBS with an Al-synergistic effect and a BS site is impossible using other techniques, such as FTIR. In flame-spray pyrolysis, the high flame temperature (~2000 K) and oxygen-rich atmosphere promote the formation of Si−O−Al bonds, leading to highly populated surface Al^{V} species and much higher BAS density than in ASAs prepared at milder conditions.[24,44] The harsh synthesis conditions using FSP provide a more homogeneous distribution of Al and Si atoms even at high Al loading, which tends to promote the formation of bridging silanol groups based on either Al^{IV} or Al^{V} sites in flame-derived ASAs. Hence, we could directly observe here that the formation of bridging SiOHAl is not a unique property of zeolites featuring long-range order but is also possible in amorphous materials, such as ASAs.

As the formation and the amount of SiOHAl sites depend on the Al/Si ratio and Al distribution, it may be possible to tune the acidity of ASAs for the selective production of middle distillates from hydrocracking. In addition, the strong SiOHAl BASs can cooperate with other sites on the surface of ASAs for the catalysis of multistep reactions, including bifunctional Brønsted-Lewis acid-catalytic glucose dehydration for 5-hydroxymethylfurfural.[56−58] Moreover, bridging OH groups could result in strong metal−support interactions,[59] enhancing the catalytic activity and stability of active metal species for removing hazardous gases, such as NO, NO_2, NH_3, and volatile organic compounds,[60,61] with benefits to the environment and human health. Therefore, our discovery of SiOHAl formation in ASAs could significantly expand their applications in various fields.

In summary, the formation of Al^{IV}-based bridging OH groups in ASAs, together with a new type of Al^{V}-based bridging OH group, is directly observed by ^{27}Al-{^{1}H} D-HMQC 2D NMR spectroscopy. So far, bridging OH groups, as the key catalytic active sites, have been widely accepted to be formed with framework Al^{IV} species in crystalline zeolites. Compared to zeolites, the formation of bridging OH groups in ASAs is strongly under debate due to the lack of long-range order in these materials, longer Al−O distance, significantly lower Brønsted acidity, and rare spectral evidence. Here, we proved the formation of bridging OH groups in ASAs based on Al^{IV} and Al^{V} species in proximity to SiOH groups, showing similar ^{1}H isotropic chemical shifts and acidic properties as those in zeolites. We demonstrated that the formation of bridging OH groups is general in silica−aluminas and virtually independent from the long-range order of the local structure. This could be achieved by reducing the distance between Al^{IV}/Al^{V} species and SiOH groups in compact structure in ASAs by using a suitable synthesis approach. Our findings, which are related to the use of a very high magnetic field (35.2 T), show promise for the development of ASAs populated with bridging OH groups, enhancing their acidity and catalytic activity for a wide range of acid and multifunctional catalysis for energy and chemical production in key industrial chemical processes.

■ ASSOCIATED CONTENT

Supporting Information

The Supporting Information is available free of charge at https://pubs.acs.org/doi/10.1021/acs.jpclett.1c02975.

Method for simulating the 1D ^{27}Al MAS NMR spectra 1D ^{27}Al and ^{1}H MAS NMR spectra ^{27}Al-{^{1}H} D-HMQC 2D spectrum of ASA/10 ^{27}Al and ^{1}H DQ-SQ 2D spectrum of ASAs ^{27}Al and ^{1}H slices from Figure 4 XRD patterns, STEM and EDX images of ASAs nitrogen adsorption/desorption isotherms of ASAs. Table S1. Summary of parameters and deconvolution results Table S2. Surface areas and acidic properties of ASA catalysts (PDF)

■ AUTHOR INFORMATION

Corresponding Authors

Olivier Lafon − *Université de Lille, CNRS, Centrale Lille, Université d' Artois, UMR 8181-UCCS-Unité de Catalyse et Chimie de Solide, F-59000 Lille, France; Institut Universitaire de France*, http://www.iufrance.fr/; orcid.org/0000-0002-5214-4060; Email: olivier.lafon@univ-lille.fr

Jun Huang − *Laboratory for Catalysis Engineering, School of Chemical and Biomolecular Engineering, The University of Sydney, Sydney, New South Wales 2006, Australia;* orcid.org/0000-0001-8704-605X; Email: jun.huang@sydney.edu.au

Authors

Zichun Wang − *Laboratory for Catalysis Engineering, School of Chemical and Biomolecular Engineering, The University of Sydney, Sydney, New South Wales 2006, Australia;*

Department of Engineering, Macquarie University, Sydney, New South Wales 2109, Australia; orcid.org/0000-0002-4280-2787

Kuizhi Chen − *National High Magnetic Field Laboratory, Tallahassee, Florida 32310, United States;* orcid.org/0000-0002-9853-7070

Yijiao Jiang − *Department of Engineering, Macquarie University, Sydney, New South Wales 2109, Australia;* orcid.org/0000-0002-6191-9825

Julien Trébosc − *Université de Lille, CNRS, Centrale Lille, Université d' Artois, UMR 8181-UCCS-Unité de Catalyse et Chimie de Solide, F-59000 Lille, France; Université de Lille, CNRS, Centrale Lille, Université d' Artois, F-59000 Lille, France*

Wenjie Yang − *Laboratory for Catalysis Engineering, School of Chemical and Biomolecular Engineering, The University of Sydney, Sydney, New South Wales 2006, Australia*

Jean-Paul Amoureux − *Université de Lille, CNRS, Centrale Lille, Université d' Artois, UMR 8181-UCCS-Unité de Catalyse et Chimie de Solide, F-59000 Lille, France; Bruker Biospin, 67166 Wissembourg, France; Riken NMR Science and Development Division, 230-0045 Kanagawa, Japan*

Ivan Hung − *National High Magnetic Field Laboratory, Tallahassee, Florida 32310, United States;* orcid.org/0000-0001-8916-739X

Zhehong Gan − *National High Magnetic Field Laboratory, Tallahassee, Florida 32310, United States;* orcid.org/0000-0002-9855-5113

Alfons Baiker − *Institute for Chemical and Bioengineering, Department of Chemistry and Applied Bioscience, ETH Zürich, HCI, CH-8093 Zürich, Switzerland;* orcid.org/0000-0003-1408-464X

Complete contact information is available at: https://pubs.acs.org/10.1021/acs.jpclett.1c02975

Author Contributions

All authors have given approval to the final version of the manuscript.

Notes

The authors declare no competing financial interest.

■ ACKNOWLEDGMENTS

J.H. and Z.W. acknowledge the financial support from the Australian Research Council Discovery Projects (DP150103842, DP180104010, and DE190101618). J.H. acknowledges the University of Sydney SOAR fellowship, Sydney Nano Grand Challenge, and the International Project Development Funding. O.L., J.H., and J.-P.A. are grateful for funding provided by the Region Nord/Pas de Calais (France), Europe (FEDER), CNRS, Ministère de l'Enseignement Supérieur et de la Recherche, CPER, Chevreul Institute (FR 2638), Infrastructure de Recherche en Résonance Magnétique Nucléaire à Très Haut Champ (IR-RMN, FR 3050), ENSCL, and contracts ANR-18-CE08-0015-01 (ThinGlass) and T-UEPEARL-20-005-LAFON-HAMDOUNA (NMR-MECA-DRUG). O.L. acknowledges financial support from Institut Universitaire de France (IUF). A portion of this work was performed at the National High Magnetic Field Laboratory, which is supported by the National Science Foundation Cooperative Agreement No. DMR-1644779 and the State of Florida. Development of the 36 T SCH magnet and NMR instrumentation was supported by NSF (DMR-1039938 and DMR-0603042) and NIH (BTRR 1P41 GM122698).

■ REFERENCES

(1) Li, Y.; Li, L.; Yu, J. H. Applications of Zeolites in Sustainable Chemistry. *Chem.* **2017**, *3*, 928−949.

(2) Corma, A. Inorganic solid acids and their use in acid-catalyzed hydrocarbon reactions. *Chem. Rev.* **1995**, *95*, 559−614.

(3) Wang, Z.; Li, T.; Jiang, Y.; Lafon, O.; Liu, Z.; Trébosc, J.; Baiker, A.; Amoureux, J.-P.; Huang, J. Acidity enhancement through synergy of penta- and tetra-coordinated aluminum species in amorphous silica networks. *Nat. Commun.* **2020**, *11*, 225.

(4) Wang, Z.; Pokhrel, S.; Chen, M.; Hunger, M.; Mädler, L.; Huang, J. Palladium-doped silica−alumina catalysts obtained from double-flame FSP for chemoselective hydrogenation of the model aromatic ketone acetophenone. *J. Catal.* **2013**, *302*, 10−19.

(5) Wang, Z.; Jiang, Y.; Baiker, A.; Huang, J. Efficient acid-catalyzed conversion of phenylglyoxal to mandelates on flame-derived silica/alumina. *ACS Catal.* **2013**, *3*, 1573−1577.

(6) Mouat, A. R.; George, C.; Kobayashi, T.; Pruski, M.; van Duyne, R. P.; Marks, T. J.; Stair, P. C. Highly dispersed SiO_x/Al_2O_3 catalysts illuminate the reactivity of isolated silanol sites. *Angew. Chem., Int. Ed.* **2015**, *54*, 13346−13351.

(7) Wang, Y. J.; Liu, C.; Wu, Y. J.; Song, Y. H.; Zhu, M. L.; Huang, J.; Liu, Z. T.; Liu, Z. W. Flame-spray-pyrolysis amorphous alumina-silica for tailoring the product distribution of Fischer−Tropsch synthesis. *Catal. Today* **2020**, *339*, 40−47.

(8) Yun, D.; Yun, Y. S.; Kim, T. Y.; Park, H.; Lee, J. M.; Han, J. W.; Yi, J. Mechanistic study of glycerol dehydration on Brønsted acidic amorphous aluminosilicate. *J. Catal.* **2016**, *341*, 33−43.

(9) Aitani, A. M. Oil Refining and Products. In *Encyclopedia of Energy*; Cleveland, C. J., Eds.; Elsevier: New York, U.S.A., 2004; pp 715−729.

(10) Chizallet, C. Toward the atomic scale simulation of intricate acidic aluminosilicate catalysts. *ACS Catal.* **2020**, *10*, 5579−5601.

(11) Busca, G. Silica-alumina catalytic materials: A critical review. *Catal. Today* **2020**, *357*, 621−629.

(12) Wang, Z.; Buechel, R.; Jiang, Y.; Wang, L.; Xu, H.; Castignolles, P.; Gaborieau, M.; Lafon, O.; Amoureux, J.-P.; Hunger, M.; Baiker, A.; Huang, J. Engineering the distinct structure interface of subnano-alumina domains on silica for acidic amorphous silica−alumina toward biorefining. *JACS Au* **2021**, *1*, 262−271.

(13) Chizallet, C.; Raybaud, P. Pseudo-bridging silanols as versatile Brønsted acid sites of amorphous aluminosilicate surfaces. *Angew. Chem., Int. Ed.* **2009**, *48*, 2891−2893.

(14) Perras, F. A.; Wang, Z.; Kobayashi, T.; Baiker, A.; Huang, J.; Pruski, M. Shedding light on the atomic-scale structure of amorphous silica-alumina and its Brønsted acid sites. *Phys. Chem. Chem. Phys.* **2019**, *21*, 19529−19537.

(15) Wang, Z. C.; Jiang, Y. J.; Lafon, O.; Trebosc, J.; Kim, K. D.; Stampfl, C.; Baiker, A.; Amoureux, J.-P.; Huang, J. Brønsted acid sites based on penta-coordinated aluminum species. *Nat. Commun.* **2016**, *7*, 13820.

(16) Luo, Q.; Deng, F.; Yuan, Z. Y.; Yang, J.; Zhang, M. J.; Yue, Y.; Ye, C. H. Using trimethylphosphine as a probe molecule to study the acid states in Al-MCM-41 materials by solid-state NMR spectroscopy. *J. Phys. Chem. B* **2003**, *107*, 2435−2442.

(17) Wang, Z.; Ling, H.; Shi, J.; Stampfl, C.; Yu, A.; Hunger, M.; Huang, J. Acidity enhanced [Al]MCM-41 via ultrasonic irradiation for the Beckmann rearrangement of cyclohexanone oxime to ε-caprolactam. *J. Catal.* **2018**, *358*, 71−79.

(18) Xu, J.; Wang, Q.; Deng, F. Metal active sites and their catalytic functions in zeolites: Insights from solid-state NMR spectroscopy. *Acc. Chem. Res.* **2019**, *52*, 2179−2189.

(19) Jiang, Y.; Huang, J.; Dai, W.; Hunger, M. Solid-state nuclear magnetic resonance investigations of the nature, property, and activity of acid sites on solid catalysts. *Solid State Nucl. Magn. Reson.* **2011**, *39*, 116−141.

(20) Bevilacqua, M.; Montanari, T.; Finocchio, E.; Busca, G. Are the active sites of protonic zeolites generated by the cavities? *Catal. Today* **2006**, *116*, 132−142.
(21) Xu, B.; Sievers, C.; Lercher, J. A.; van Veen, J. A. R.; Giltay, P.; Prins, R.; van Bokhoven, J. A. Strong Brønsted acidity in amorphous silica−aluminas. *J. Phys. Chem. C* **2007**, *111*, 12075−12079.
(22) Poduval, D. G.; van Veen, J. A. R.; Rigutto, M. S.; Hensen, E. J. M. Brønsted acid sites of zeolitic strength in amorphous silica-alumina. *Chem. Commun.* **2010**, *46*, 3466−3468.
(23) Xu, J.; Wang, Q.; Li, S.; Deng, F. Solid-state NMR characterization of acid properties of zeolites and solid acid catalysts. In *Solid-State NMR in Zeolite Catalysis*; Springer: Singapore, 2019; pp 159−197.
(24) Wang, Z.; Jiang, Y.; Jin, F.; Stampfl, C.; Hunger, M.; Baiker, A.; Huang, J. Strongly enhanced acidity and activity of amorphous silica−alumina by formation of pentacoordinated Al^{V} species. *J. Catal.* **2019**, *372*, 1−7.
(25) Wang, Z.; Jiang, Y.; Rachwalik, R.; Liu, Z.; Shi, J.; Hunger, M.; Huang, J. One-step room-temperature synthesis of [Al]MCM-41 materials for the catalytic conversion of phenylglyoxal to ethylmandelate. *ChemCatChem* **2013**, *5*, 3889−3896.
(26) Deng, F.; Yue, Y.; Ye, C. H. $^{1}H/^{27}Al$ TRAPDOR NMR studies on aluminum species in dealuminated zeolites. *Solid State Nucl. Magn. Reson.* **1998**, *10*, 151−160.
(27) Grey, C. P.; Vega, A. J. Determination of the quadrupole coupling constant of the invisible aluminum spins in zeolite HY with $^{1}H/^{27}Al$ TRAPDOR NMR. *J. Am. Chem. Soc.* **1995**, *117*, 8232−8242.
(28) Perras, F. A.; Kobayashi, T.; Pruski, M. Natural abundance ^{17}O DNP two-dimensional and surface-enhanced NMR spectroscopy. *J. Am. Chem. Soc.* **2015**, *137*, 8336−8339.
(29) Liao, W. C.; Ghaffari, B.; Gordon, C. P.; Xu, J.; Copéret, C. Dynamic nuclear polarization surface enhanced NMR spectroscopy (DNP SENS): Principles, protocols, and practice. *Curr. Opin. Colloid Interface Sci.* **2018**, *33*, 63−71.
(30) Chen, K.; Horstmeier, S.; Nguyen, V. T.; Wang, B.; Crossley, S. P.; Pham, T.; Gan, Z.; Hung, I.; White, J. L. Structure and catalytic characterization of a second framework Al(IV) site in zeolite catalysts revealed by NMR at 35.2 T. *J. Am. Chem. Soc.* **2020**, *142*, 7514−7523.
(31) Kaushik, M.; Leroy, C.; Chen, Z.; Gajan, D.; Willinger, E.; Müller, C. R.; Fayon, F.; Massiot, D.; Fedorov, A.; Copéret, C.; Lesage, A.; Florian, P. Atomic-scale structure and its impact on chemical properties of aluminum oxide layers prepared by atomic layer deposition on silica. *Chem. Mater.* **2021**, *33*, 3335−3348.
(32) Yang, W.; Wang, Z.; Huang, J.; Jiang, Y. Qualitative and quantitative analysis of acid properties for solid acids by solid-state nuclear magnetic resonance spectroscopy. *J. Phys. Chem. C* **2021**, *125*, 10179−10197.
(33) Jiao, J.; Kanellopoulos, J.; Wang, W.; Ray, S. S.; Foerster, H.; Freude, D.; Hunger, M. Characterization of framework and extra-framework aluminum species in non-hydrated zeolites Y by ^{27}Al spin-echo, high-speed MAS, and MQMAS NMR spectroscopy at $B_0 = 9.4$ to 17.6 T. *Phys. Chem. Chem. Phys.* **2005**, *7*, 3221−3226.
(34) Huang, J.; van Vegten, N.; Jiang, Y.; Hunger, M.; Baiker, A. Increasing the Brønsted acidity of flame-derived silica/alumina up to zeolitic strength. *Angew. Chem., Int. Ed.* **2010**, *49*, 7776−7781.
(35) Wang, Z.; Jiang, Y.; Stampfl, C.; Baiker, A.; Hunger, M.; Huang, J. NMR spectroscopic characterization of flame-made amorphous silica-alumina for cyclohexanol and glyceraldehyde conversion. *ChemCatChem* **2020**, *12*, 287−293.
(36) Harris, R. K.; Becker, E. D.; Cabral de Menezes, S. M.; Goodfellow, R.; Granger, P. NMR nomenclature: Nuclear spin properties and conventions for chemical shifts: IUPAC recommendations 2001. *Solid State Nucl. Magn. Reson.* **2002**, *22*, 458−483.
(37) Massiot, D.; Touzo, B.; Trumeau, D.; Coutures, J. P.; Virlet, J.; Florian, P.; Grandinetti, P. J. Two-dimensional magic-angle spinning isotropic reconstruction sequences for quadrupolar nuclei. *Solid State Nucl. Magn. Reson.* **1996**, *6*, 73−83.
(38) Hung, I.; Trébosc, J.; Hoatson, G. L.; Vold, R. L.; Amoureux, J.-P.; Gan, Z. Q-shear transformation for MQMAS and STMAS NMR spectra. *J. Magn. Reson.* **2009**, *201*, 81−86.
(39) Wang, Q.; Hu, B.; Lafon, O.; Trébosc, J.; Deng, F.; Amoureux, J.-P. Double-quantum homonuclear NMR correlation spectroscopy of quadrupolar nuclei subjected to magic-angle spinning and high magnetic field. *J. Magn. Reson.* **2009**, *200*, 251−260.
(40) Siegel, R.; Nakashima, T. T.; Wasylishen, R. E. Signal enhancement of NMR spectra of half-integer quadrupolar nuclei in solids using hyperbolic secant pulses. *Chem. Phys. Lett.* **2004**, *388*, 441−445.
(41) Yao, Z.; Kwak, H.-T.; Sakellariou, D.; Emsley, L.; Grandinetti, P. J. Sensitivity enhancement of the central transition NMR signal of quadrupolar nuclei under magic-angle spinning. *Chem. Phys. Lett.* **2000**, *327*, 85−90.
(42) Kwak, H. T.; Prasad, S.; Clark, T.; Grandinetti, P. J. Enhancing sensitivity of quadrupolar nuclei in solid-state NMR with multiple rotor assisted population transfers. *Solid State Nucl. Magn. Reson.* **2003**, *24*, 71−77.
(43) Brinkmann, A.; Kentgens, A. P. M. Proton-selective $^{17}O-^{1}H$ distance measurements in fast magic-angle-spinning solid-state NMR spectroscopy for the determination of hydrogen bond lengths. *J. Am. Chem. Soc.* **2006**, *128*, 14758−14759.
(44) Wang, Z.; Jiang, Y.; Yi, X.; Zhou, C.; Rawal, A.; Hook, J.; Liu, Z.; Deng, F.; Zheng, A.; Hunger, M.; Baiker, A.; Huang, J. High population and dispersion of pentacoordinated Al^{V} species on the surface of flame-made amorphous silica-alumina. *Sci. Bull.* **2019**, *64*, 516−523.
(45) Kim, K. D.; Pokhrel, S.; Wang, Z. C.; Ling, H. J.; Zhou, C. F.; Liu, Z. W.; Hunger, M.; Mädler, L.; Huang, J. Tailoring high-performance Pd catalysts for chemoselective hydrogenation reactions via optimizing the parameters of the double-flame spray pyrolysis. *ACS Catal.* **2016**, *6*, 2372−2381.
(46) Jiao, J.; Kanellopoulos, J.; Behera, B.; Jiang, Y. J.; Huang, J.; Marthala, V. R. R.; Ray, S. S.; Wang, W.; Hunger, M. Effects of adsorbate molecules on the quadrupolar interaction of framework aluminum atoms in dehydrated zeolite H, Na-Y. *J. Phys. Chem. B* **2006**, *110*, 13812−13818.
(47) Wang, Q.; Li, W.; Hung, I.; Mentink-Vigier, F.; Wang, X.; Qi, G.; Wang, X.; Gan, Z.; Xu, J.; Deng, F. Mapping the oxygen structure of γ-Al_2O_3 by high-field solid-state NMR spectroscopy. *Nat. Commun.* **2020**, *11*, 3620.
(48) Valla, M.; Rossini, A. J.; Caillot, M.; Chizallet, C.; Raybaud, P.; Digne, M.; Chaumonnot, A.; Lesage, A.; Emsley, L.; van Bokhoven, J. A.; Coperet, C. Atomic description of the interface between silica and alumina in aluminosilicates through dynamic nuclear polarization surface-enhanced NMR spectroscopy and First-Principles calculations. *J. Am. Chem. Soc.* **2015**, *137*, 10710−10719.
(49) Hunger, M.; Freude, D.; Pfeifer, H. Magic-angle spinning nuclear-magnetic-resonance studies of water-molecules adsorbed on Brønsted-acid and Lewis-acid sites in zeolites and amorphous silica-aluminas. *J. Chem. Soc., Faraday Trans.* **1991**, *87*, 657−662.
(50) Batista, A. T. F.; Wisser, D.; Pigeon, T.; Gajan, D.; Diehl, F.; Rivallan, M.; Catita, L.; Gay, A.-S.; Lesage, A.; Chizallet, C.; Raybaud, P. Beyond γ-Al_2O_3 crystallite surfaces: The hidden features of edges revealed by solid-state ^{1}H NMR and DFT calculations. *J. Catal.* **2019**, *378*, 140−143.
(51) Lang, S.; Benz, M.; Obenaus, U.; Himmelmann, R.; Hunger, M. Novel approach for the characterization of Lewis acidic solid catalysts by solid-state NMR spectroscopy. *ChemCatChem* **2016**, *8*, 2031−2036.
(52) Yin, F.; Blumenfeld, A. L.; Gruver, V.; Fripiat, J. J. NH_3 as a probe molecule for NMR and IR study of zeolite catalyst acidity. *J. Phys. Chem. B* **1997**, *101*, 1824−1830.
(53) Ma, D.; Han, X. W.; Xie, S. J.; Bao, X. H.; Hu, H. B.; Au-Yeung, S. C. F. An investigation of the roles of surface aluminum and acid sites in the zeolite MCM-22. *Chem. - Eur. J.* **2002**, *8*, 162−170.
(54) Chizallet, C.; Raybaud, P. Acidity of amorphous silica-alumina: From coordination promotion of Lewis sites to proton transfer. *ChemPhysChem* **2010**, *11*, 105−108.

https://doi.org/10.1021/acs.jpclett.1c02975
J. Phys. Chem. Lett. 2021, 12, 11563−11572

(55) Chizallet, C.; Raybaud, P. Density functional theory simulations of complex catalytic materials in reactive environments: Beyond the ideal surface at low coverage. *Catal. Sci. Technol.* **2014**, *4*, 2797−2813.
(56) Wang, Z.; Wang, L.; Jiang, Y.; Hunger, M.; Huang, J. Cooperativity of Brønsted and Lewis acid sites on zeolite for glycerol dehydration. *ACS Catal.* **2014**, *4*, 1144−1147.
(57) Wang, C.; Chu, Y.; Xu, J.; Wang, Q.; Qi, G.; Gao, P.; Zhou, X.; Deng, F. Extra-framework aluminum-assisted initial C−C bond formation in methanol-to-olefins conversion on zeolite H-ZSM-5. *Angew. Chem., Int. Ed.* **2018**, *57*, 10197−10201.
(58) Wang, Z.; O'Dell, L. A.; Zeng, X.; Liu, C.; Zhao, S.; Zhang, W.; Gaborieau, M.; Jiang, Y.; Huang, J. Insight into three-coordinate aluminum species on ethanol-to-olefin conversion over ZSM-5. *Angew. Chem., Int. Ed.* **2019**, *58*, 18061−18068.
(59) Mojet, B. L.; Kappers, M. J.; Miller, J. T.; Koningsberger, D. C. Metal-support interactions in supported platinum catalysts: zeolites and amorphous supports. *Stud. Surf. Sci. Catal.* **1996**, *101*, 1165−1174.
(60) Ma, L.; Cheng, Y.; Cavataio, G.; McCabe, R. W.; Fu, L.; Li, J. *In situ* DRIFTS and temperature-programmed technology study on NH_3-SCR of NO_x over Cu-SSZ-13 and Cu-SAPO-34 catalysts. *Appl. Catal., B* **2014**, *156−157*, 428−437.
(61) Zhang, R.; Liu, N.; Lei, Z.; Chen, B. Selective transformation of various nitrogen-containing exhaust gases toward N_2 over zeolite catalysts. *Chem. Rev.* **2016**, *116*, 3658−3721.

https://doi.org/10.1021/acs.jpclett.1c02975
J. Phys. Chem. Lett. 2021, 12, 11563−11572